Electronic Supplementary Material (ESI) for Reaction Chemistry & Engineering.

Supporting Information

Co_3O_4 supported by ultrathin-layered graphitic carbon nitride for efficient electrocatalytic evolution of oxygen

Ruixue Luo[a], Xi Li[a], Youping Guo[a] and Renchun Fu*[a]

The correlation of the Tafel slope, overpotential and current density

The Tafel slope is an important kinetic parameter in the electrolytic water reaction process, which is used to express the sensitivity of the reaction pathway and reaction potential relative to the electrode potential[1]. the Tafel slope is an inherent property of the electrode material itself, and the magnitude of the Tafel slope value is closely related to the electrolytic water reaction rate in the actual electrolytic water reaction process. in order to make the reaction current density (j_0) increases, it is necessary to apply a high overpotejntial (η), the expressions are shown below:

$$\eta = a + b\log(j_0) \quad \text{(Eq. S1)}$$

where η is the overpotential, a is a constant, b is the Tafel slope, and j_0 is the exchange current density. In general, if the overpotential (η) is smaller, the corresponding current density (j) grows faster. The current density (j) and overpotential can be described by the known Butler-Volmer equation[2, 3]:

$$j = j_0[\exp(\frac{\alpha_a naF\eta}{RT}) + \exp(\frac{-\alpha_c naF\eta}{RT})] \quad \text{(Eq. S2)}$$

In the above equation, j is the current density, j_0 is the exchange current density, α is the charge transfer coefficient, n is the number of electrons transferred during the electrode reaction, F is the Faraday constant, η is the activation overpotential, R is the ideal gas constant, T represents the Kelvin temperature of the reaction, and the charge transfer coefficient is defined as the proportion of electrical energy used to change the electrochemical reaction rate, and the charge transfer coefficient is controlled by the electron transfer at the electrode electrolyte nterface The charge transfer coefficient is controlled by the electron transfer at the electrode electrolyte interface[4]. Where α_a is the reduction charge transfer coefficient and α_a is the oxidation charge transfer coefficient. However, in the specific reaction process, the exact reaction mechanism is difficult to determine, and if the reaction mechanism has been determined, the charge transfer coefficient can be expressed as follows[5]:

$$\alpha_a = \frac{n-\gamma}{v} - s\beta \quad \text{(Eq. S3)}$$

$$\alpha_c = \frac{\gamma}{v} + s\beta \quad \text{(Eq. S4)}$$

In the above equation, n is the total number of electrons transferred in the reaction, γ is the number of electrons transferred before the confirmatory step, v is the number of confirmatory steps occurring in one reaction during the whole reaction, s is the number of electrons transferred in the confirmatory step and β is the symmetry factor. Then equation (3) is simplified and equation (3) is expressed as follow[6]:

$$j = j_0(\exp[\frac{(1-\beta)F\eta}{RT}] - \exp[\frac{-\beta F\eta}{RT}]) \quad \text{(Eq. S5)}$$

The Butler-Volmer equation is the sum of the anodic current density (and cathodic current density. However, under high anodic overpotential conditions, the overall current comes mainly from the anodic end, while the

contribution of the cathodic part is negligible. Therefore, the Butler-Volmerr equation can be simplified as:

$$j \approx j_0 \exp \frac{\alpha_a nF\eta}{RT} \quad \text{(Eq. S6)}$$

The Tafel equation is obtained by converting the above equation into logarithmic functional form, as shown below:

$$\log(j) = \log(j_0) + \frac{\eta}{b} \text{ or } \eta = a + b\log(\frac{j}{j_0}) \quad \text{(Eq. S7)}$$

Connection between cyclic voltammetric curves and electrochemically active surface area

The electrochemical active surface area (ECSA) reflects the catalytic reaction area of the catalyst, the number of active sites in the catalyst can be obtained from the ECSA. For electrode materials with high catalytic activity, the value of ECSA is also larger. Since the bilayer capacitance (C_{dl}) of a catalyst is positively correlated with its ECSA, the size of its ECSA is usually determined based on the C_{dl} value of the catalyst. The value of C_{dl} is first determined by performing cyclic voltammetry tests at different scan rates in the potential range of the non-electrochemical reaction, and based on the test results, the difference between the corresponding current density at a certain potential ($\Delta j = j_a - j_c$), where , j_a and j_c are the anodic and cathodic current densities, respectively)[7], plotted with the scan rate as the variable, and fitted to obtain half of the slope of the line as the C_{dl} value of the catalyst. the relationship between ECSA and C_{dl} can be calculated by the following equation:

$$ECSA = C_{dl} / C_S \quad \text{(S8)}$$

Where C_S is the specific capacitance. In order to determine ECSA, the value of the specific capacitance (C_S) needs to be determined.Where C_S is the specific capacitance of a flat surface with 1 cm2 of real surface area. Here we assume its value is 40 μF·cm^{-2} per for the flat electrode[8].

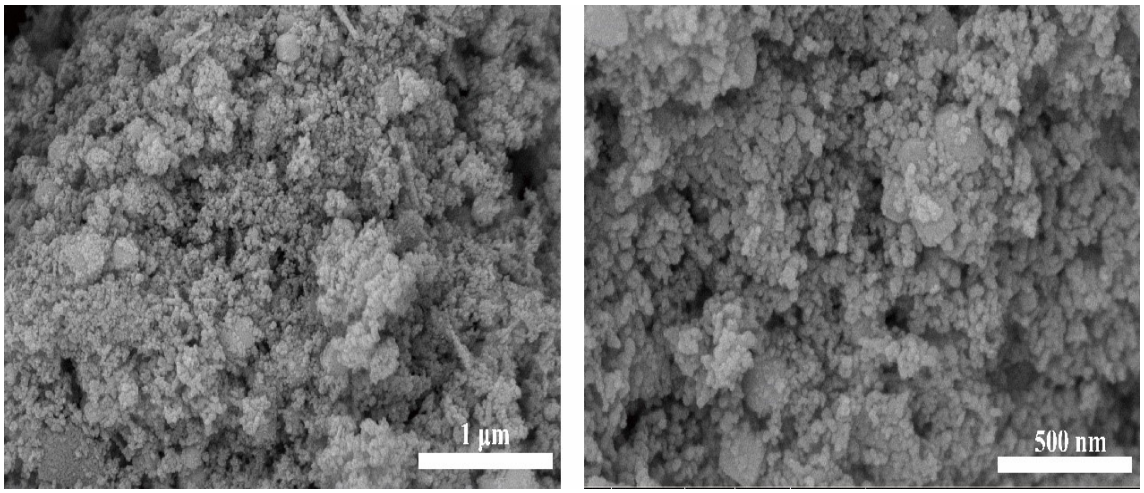

Fig S1. SEM images of pristine Co_3O_4 with different magnifications.

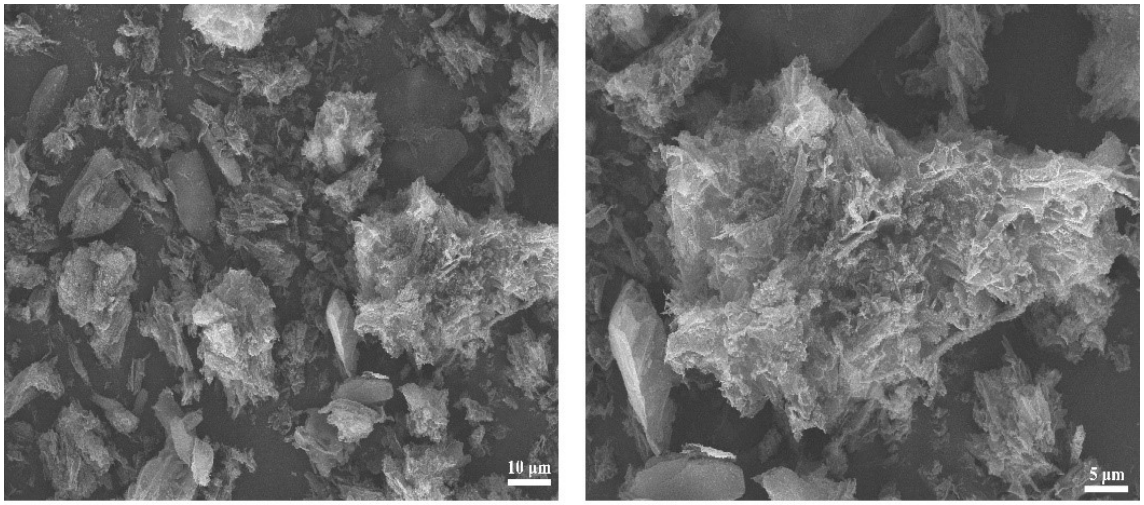

Fig S2.SEM images of pristine g-C_3N_4 with different magnifications.

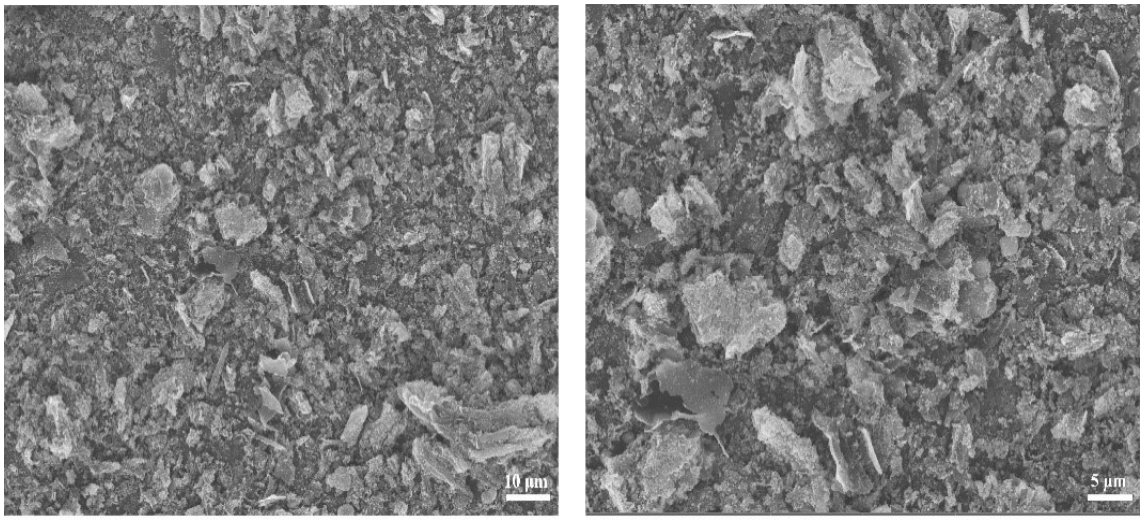

Fig S3.SEM images of Co_3O_4@g-C_3N_4 composite material with different magnifications.

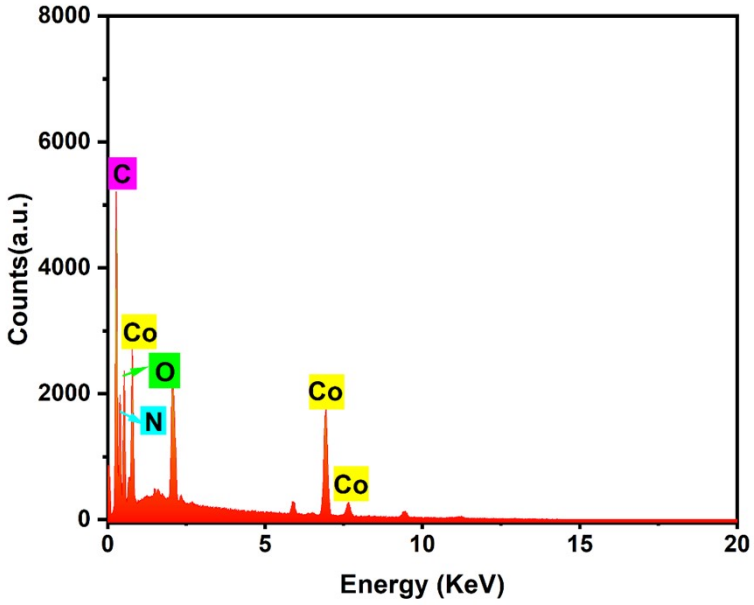

Fig S4. The EDS spectroscop results of Co_3O_4@g-C_3N_4 composites.

Table S1. Quantitative results for C, N, O, and Co in Co_3O_4@g-C_3N_4 from EDS.

element	wt%	wt% sigma	At%
C	37.80	0.36	49.72
N	27.10	0.48	30.58
O	14.30	0.24	14.12
Co	20.80	0.24	5.58
Total	100.00		100.00

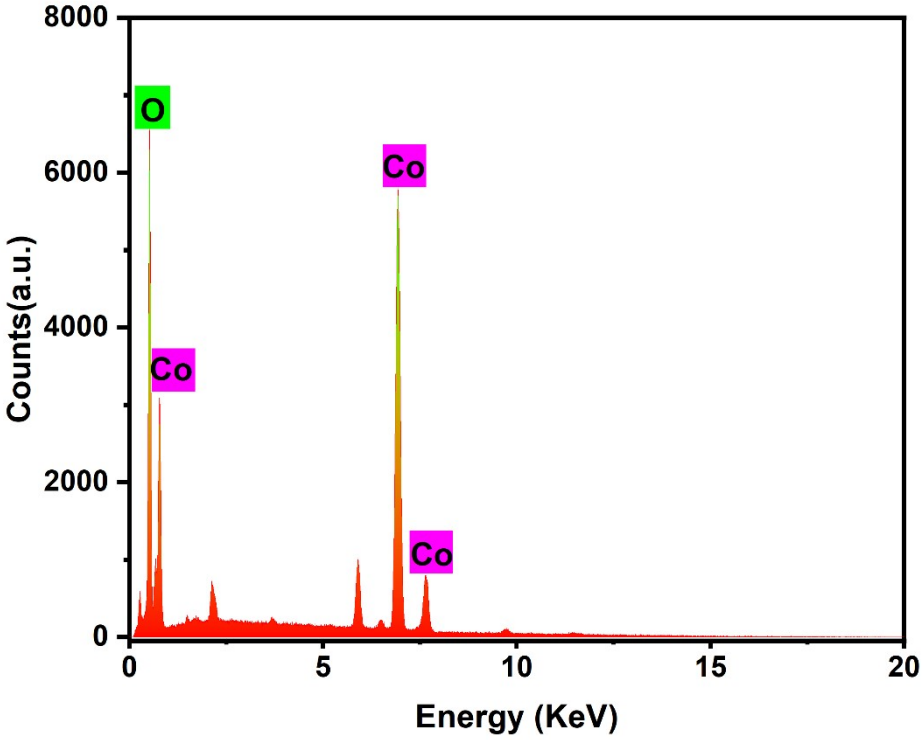

Fig S5. The EDS spectroscop results of pristine Co_3O_4.

Table S2. Quantitative results for O and Co in Co_3O_4 from EDS.

element	wt%	wt% sigma	At%
O	18.83	0.11	47.02
Co	69.02	0.66	49.79
Total	87.85		96.81

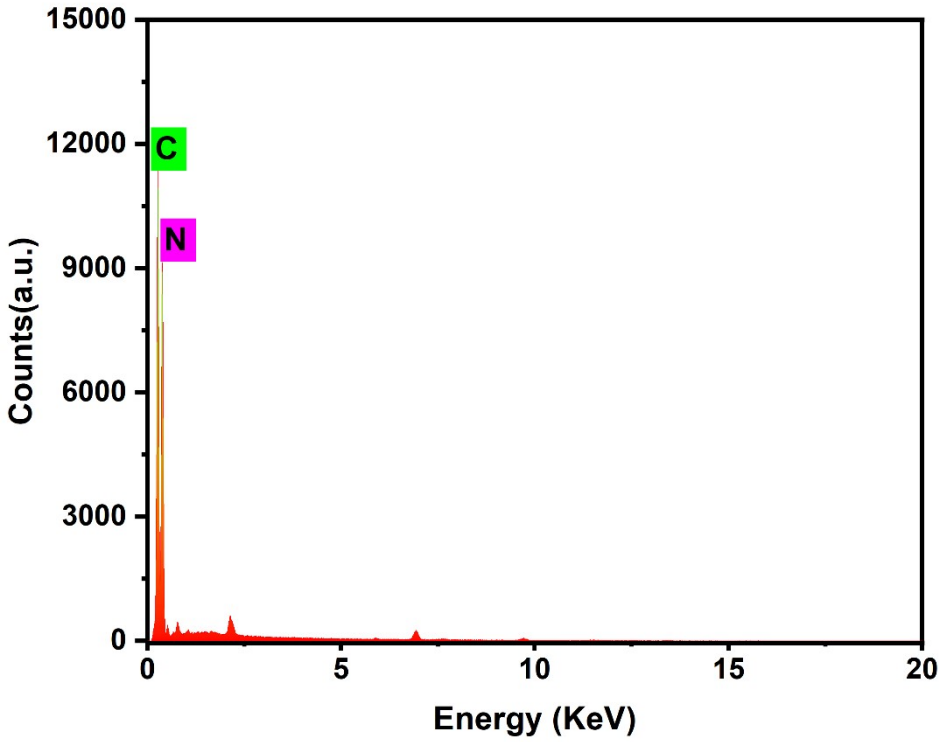

Fig S6. The EDS spectroscop results of g-C_3N_4.

Table S3. Quantitative results for C N in g-C_3N_4 from EDS.

element	wt%	wt% sigma	At%
C	36.11	0.25	39.76
N	63.02	0.26	59.51
Total	99.13		99.27

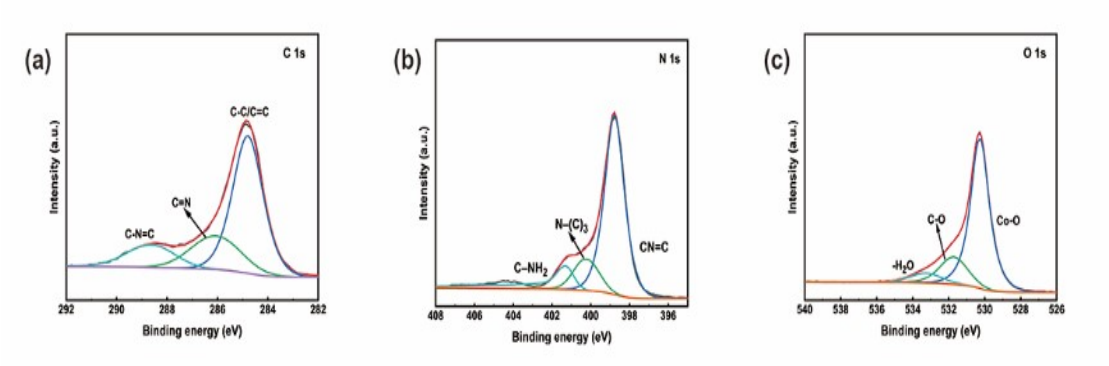

Fig S7. High-resolution XPS spectra of (a) C 1s region of g-C_3N_4 composites, (b) N 1s region of g-C_3N_4 composites, (c) O 1s region of Co3O4.

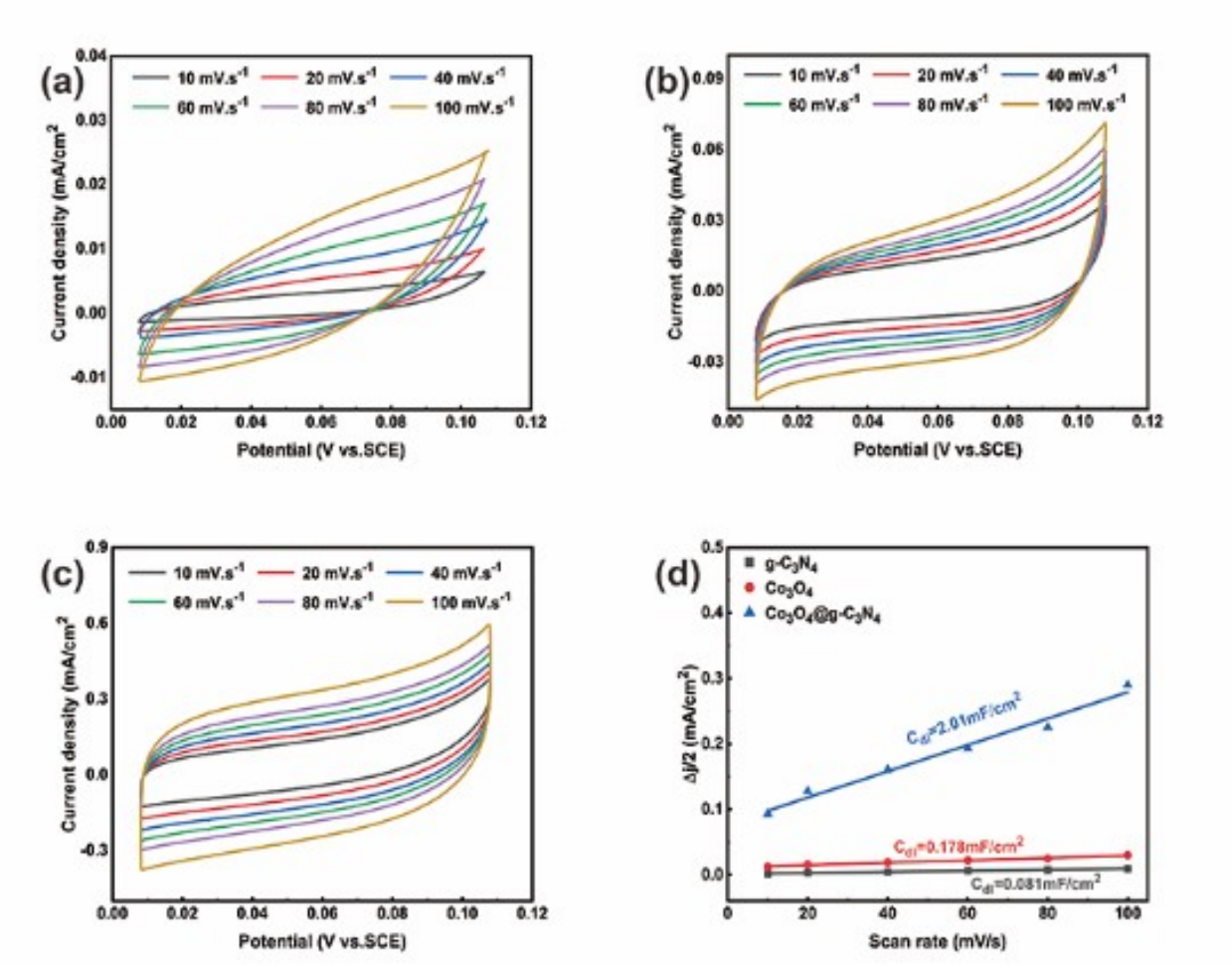

Fig S8. Cyclic voltammetry curves of (a) g-C_3N_4, (b) Co_3O_4, (c) Co_3O_4/gC_3N_4, (d) double layer capacitance (Cdl) of the catalysts.

Table S4. Summary of electrochemical OER activity of catalyst.

simple	Overpotential η10 (mV)	Tafel slop ($mV.dec^{-1}$)	Mass loading (mg/cm^2)	Cdl (mF/cm^2)	ECSA(mF/cm^2)
g-C_3N_4	N/A	451.01	1.2	0.081	~2.025
Co_3O_4	430	132.09	1.4	0.178	~4.45
Co_3O_4@g-C_3N_4	340	120.92	1.1	2.01	~50.25
CP	480	215.24	N/A	N/A	N/A
Pt	600	129.21	N/A	N/A	N/A

Table S5. OER poteals of the prepared catalysts comparison with some best reported.

Sample Name	Potentials η10 [V]	Overpotential η10 [V]	References
Co_3O_4@g-C_3N_4	1.605	0.340	This Work
Co_3O_4	1.691	0.430	This Work
*g-C_3N_4	N/A	N/A	This Work
RuO2	1.550	0.320	[9]
IrO_2	1.650	0.420	[10]
Co_3O_4/N-doped-graphene	1.540	0.310	[11]
$Ni(OH)_2$	1.590	0.360	[12]
$Co(OH)_2$@g-C_3N_4-5	1.550	0.320	[10]
Co_3O_4/P-CN	1.658	0.428	[13]
Co_3O_4@BP	1.63	0.400	[14]
Co_3O_4/MoO_3/g-C_3N_4	1.436	0.206	[7]

*g-C_3N_4 did not reach at 10 $mA \cdot cm^{-2}$ in this work.

Table S6. Peak table of Co_3O_4@g-C_3N_4 composites from XPS result.

sample	Start BE	Peak BE	End BE	Height CPS	FWHM eV	Area(P) CPS.eV	Area (N) TPP-2M	Atomic
O 1s	544.98	529.95	525.18	82252.74	1.52	181482.74	1051.2	18.48%
C 1s	297.98	288.07	279.18	56209.45	1.44	167453.45	2353.02	41.37%
Co 2p	814.98	780.02	765.18	62258.17	2.88	387578.48	444.32	7.81%
N 1s	409.98	398.61	392.18	92042.41	1.59	203761.62	1839.68	32.34%

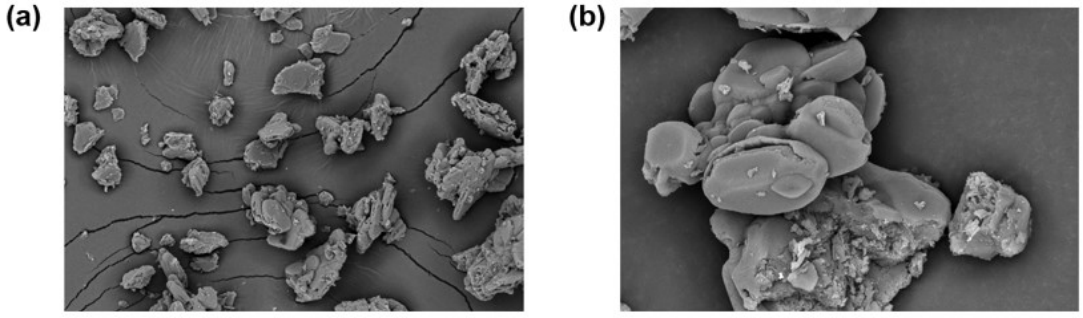

Fig S9. SEM images of (a) 500-g-C3N4 nanosheets.(b) 600-g-C3N4 nanosheets.

1. A. R. Zeradjanin, J. Masa, I. Spanos and R. Schlögl, *Frontiers in Energy Research*, 2021, **8**.
2. H. Kazemi Esfeh and M. K. A. Hamid, *Journal of Electrochemical Energy Conversion and Storage*, 2016, **13**.
3. C. Schluckner, V. Subotić, V. Lawlor and C. Hochenauer, *International Journal of Hydrogen Energy*, 2014, **39**, 19102-19118.
4. P. Yang, H. Zhang and Z. Hu, *International Journal of Hydrogen Energy*, 2016, **41**, 3579-3590.
5. D. A. Noren and M. A. Hoffman, *Journal of Power Sources*, 2005, **152**, 175-181.
6. C. Thanomjit, Y. Patcharavorachot, P. Ponpesh and A. Arpornwichanop, *International Journal of Hydrogen Energy*, 2015, **40**, 6950-6958.
7. I. Ahmed, R. Biswas, R. A. Patil, K. K. Halder, H. Singh, B. Banerjee, B. Kumar, Y.-R. Ma and K. K. Haldar, *ACS Applied Nano Materials*, 2021, **4**, 12672-12681.
8. H. Deng, C. Zhang, Y. Xie, T. Tumlin, L. Giri, S. P. Karna and J. Lin, *Journal of Materials Chemistry A*, 2016, **4**, 6824-6830.
9. L. Zhang, X. Gan, X. Zhong, L. Wang, G. Feng, L. Wang, Y. Wang, X. Lv, W. Zhu and B. Zhang, *Nanotechnology*, 2022, **33**.
10. M. Tahir, N. Mahmood, L. Pan, Z.-F. Huang, Z. Lv, J. Zhang, F. K. Butt, G. Shen, X. Zhang, S. X. Dou and J.-J. Zou, *Journal of Materials Chemistry A*, 2016, **4**, 12940-12946.
11. Y. Liang, Y. Li, H. Wang, J. Zhou, J. Wang, T. Regier and H. Dai, *Nature materials*, 2011, **10**, 780-786.
12. X.-Y. Yu, Y. Feng, B. Guan, X. W. Lou and U. Paik, *Energy & Environmental Science*, 2016, **9**, 1246-1250.
13. M. Zhu, S. Yu, R. Ge, L. Feng, Y. Yu, Y. Li and W. Li, *ACS Applied Energy Materials*, 2019, **2**, 4718-4729.
14. F. Shi, K. Huang, Y. Wang, W. Zhang, L. Li, X. Wang and S. Feng, *ACS Appl Mater Interfaces*, 2019, **11**, 17459-17466.